



Chlorella sensors in liquid marbles and droplets

Neil Phillips^{*}, Richard Mayne, Andrew Adamatzky

Unconventional Computing Laboratory, Faculty of Environment and Technology, University of the West of England, Bristol BS16 1QY, UK

ARTICLE INFO

Keywords:

Chlorella
Bio-sensor
Electrical activity

ABSTRACT

The use of live organisms in electrically-coupled sensing devices has been suggested as an alternative low-cost, low-environmental footprint and robust technology for continuous monitoring and sensing applications. The utility of *Chlorella vulgaris* algae as living biosensor media inside liquid marbles (LMs), micro-wells and surface recesses is here explored, through noninvasive measurement of electrical activity via indirect monitoring of culture media. We present results demonstrating the suitability of this organism in several experimental setups which may be adapted to a wide range of applications, and evaluate how to maximise sensing performance through optimising electrode geometry, environmental controls and, in the case of LMs, coating parameters. We conclude by discussing potential applications and further optimisations.

1. Background

Nature has provided, via evolution, efficient and robust processes for living organisms to sense their environment to increase their ability to survive and reproduce in different surroundings [1]. Biosensors based on living organisms have potential advantages over solid-state sensors including self-repair, replication, reconfigurability, lower power consumption, low environmental impact and lower financial cost. Although their use is widespread, operating solid-state sensors in hostile environments has shown they have practical issues, such as longevity [2] and robustness [2,3] which can require them to be periodically re-calibrated [4,5] or replaced [6].

Algal biosensors utilise live algae as the primary sensing component. Although they are not yet widely used in commercial settings, several studies have demonstrated their suitability for continuous monitoring applications, such as in the agro-environmental industry [7,8]. Such devices do have drawbacks, however, such as maintenance of culture environments [9] and the development of robust bio-organic interfaces [10].

The following investigation was conducted towards developing a low-cost algal biosensor with multiple, broad-spectrum uses, through experimenting with multiple culture environments and a simple, reconfigurable interface [11].

Chlorella vulgaris, further called 'Chlorella', is a planktonic unicellular green alga that forms single, spherical cells [12], which only requires sunlight, carbon dioxide and a comparatively simple nutritional medium [13]. We selected Chlorella for the following experimental

study for four primary reasons: (a) photosensitivity resulting from photosynthetic mechanisms, (b) photosynthetic activity may be measured indirectly through electrical measurement of the surrounding culture media [14], (c) robustness to changing environmental conditions [15,16], (d) rapid cell replication under preferable conditions, with a doubling time of approximately 2.5–8.0 h depending on the strain, environment and culture conditions [17].

In our previous studies [18–22] we demonstrated Liquid Marbles (LMs) have potential advantages for a diverse range of applications including those in the field of microfluidics [23,24]. These include rapid blood-typing assays [25], control of micro-encapsulated reactions [19,20] and unconventional computation signals [21,22,26]. In the following investigation, we measure the electrical activity of Chlorella in a range of experimental environments, including LMs, and evaluate which methods and materials are the most effective. For our purposes, the 'effectiveness' of a biosensor was determined through cost, ease of fabrication and maintenance, and suitability for supporting the continuous measurement of bio-electrical phenomena in an aqueous medium.

2. Methods

2.1. Algal culture

A program of experiments were conducted to explore and optimise the measurement of electrical potentials from Chlorella cells inside small (30 μ L to 150 μ L), constrained boundaries (plastic and powder walls). For experimental flexibility and measurement consistency, initial

^{*} Corresponding author.

E-mail address: neil.phillips@uwe.ac.uk (N. Phillips).

<https://doi.org/10.1016/j.sbsr.2022.100491>

Received 22 September 2021; Received in revised form 15 February 2022; Accepted 18 March 2022

Available online 23 March 2022

2214-1804/© 2022 The Authors. Published by Elsevier B.V. This is an open access article under the CC BY license (<http://creativecommons.org/licenses/by/4.0/>).

experiments were conducted inside micro-wells of the dimensions and materials found in conventional 96-well cell culture plates: open-bottom 8-well strips (Caplugs Evergreen Ltd, USA) with an internal diameter ~ 6 mm, depth 11 mm, maximum volume ~ 200 μL , recommended working volume ~ 150 μL . The environment permitted transmitted light through its transparent walls. These micro-wells were attached to bespoke printed circuit boards (PCBs) with two part-epoxy (Araldite, Huntsman Advanced Materials, UK) and closed with tapered silicon bungs (4 to 8 mm diameter, length trimmed to provide the desired volume of liquid in well). A blunt needle (18G) was inserted in parallel with bung to allow trapped air to vent and then removed.

C. vulgaris cells (Blades Biological Ltd, UK, code LZA 070) were grown in deionised water containing 2% concentration of freshwater nutrient solution Bold Modified Basal Salt (Sigma-Aldrich, UK, code B5282-500ML). The growth tank was periodically illuminated with an LED growth lamp (see Appendix A). When a density of $\sim 10 \times 10^6$ cells per ml was achieved, as determined by manual cell counts, cells were extracted for use in laboratory tests. All experiments were conducted at room temperature (18 °C to 22 °C). Chlorella cells in solution were centrifuged to increase the density of cells to $\sim 5 \times 10^8$ cells per ml (see Appendix B).

2.2. Measuring response to light in micro-wells with two pairs of electrodes

A micro-pipette was used to transfer 150 μL from the bottom of the centrifuge tube to the micro-well (allowing space for silicon bung). Each micro-well was equipped with two pairs of electrodes, one pair across the 'top' (needle electrodes, stainless steel, 0.45 mm diameter, through the silicon bung) and one pair across the 'bottom' (platinum wires, 0.3 mm diameter, soldered to PCB see Fig. 1(a)). The electrode pairs were set at 90 degrees to each other to avoid possible physical contact and minimise electrical interaction, see Fig. 1(b). This allowed electrical

potential across the top and bottom regions of the micro-well to be independently and simultaneously measured. To maximise signal to noise ratio the bespoke PCBs were designed with ground planes and connected to precision data loggers (ADC-24, PICO Technology Ltd, UK) via shielded coaxial cables with SubMiniature version A (SMA) connectors. The screw connectors on ADC-24 Terminal Board were replaced with SMA connectors, see Fig. 1(e).

The electrical potential across the two pairs of electrodes was recorded for between 1 to 5 days, sample rate 1 Hz, with and without illumination (~ 1000 lx from full spectrum LED growth lamp, colour ratio red (630–660 nm): blue (450–460 nm): orange (610–615 nm) = 7:1:1, on a mechanical timer). Experiments were repeated a minimum of 5 times per condition. Control experiments consisted of using the same measurement conditions as for Chlorella samples, but using de-ionised water and a clean growth medium.

Data were analysed using custom software, written in Python and based on the open-source SciPy library signal processing functions [27]. Outliers in both spike amplitude and duration data were removed by calculation of Z-scores and identifying points exceeding three standard deviations from the mean. Data were IRC filtered before the peak detection algorithm was applied. Normality tests were conducted using DAgostino and Pearsons combined test for skewness and kurtosis. Spike detection was autoscaled to only identify spikes as peaks if their prominence was at least 10% the magnitude of the largest peak, such that differences in amplitude resulting from differing resistances of growth media between electrodes of different separations would not affect the sensitivity of the measurement. The following characteristics were recorded for each peak: amplitude, duration, x-axis location and peak-to-peak interval. Descriptive statistics were then generated and means of spike amplitude and duration were compared within groups with a Kruskal-Wallis H-test.

The number of spikes generated for each electrode spacing was compared using Pearson's Chi-square test. In addition, clustering

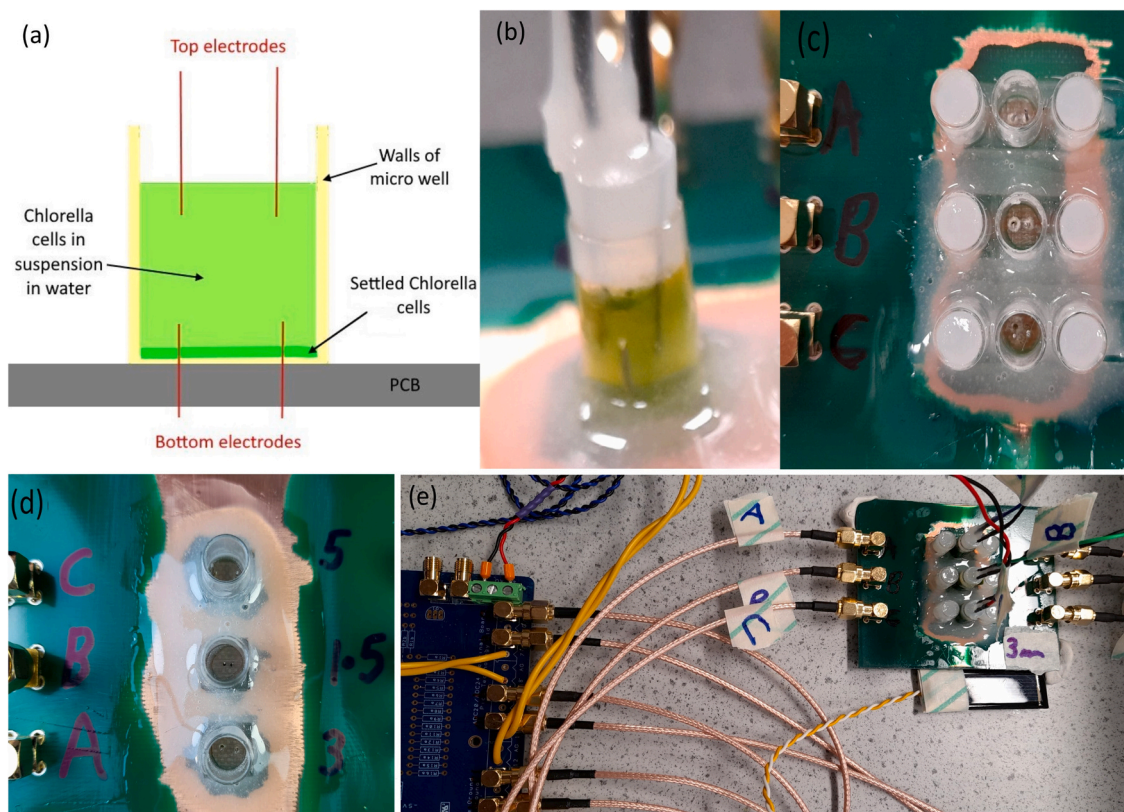


Fig. 1. Electrodes and instrumentation setup in micro-wells.

analysis via projection into two and three dimensions with Uniform Manifold Approximation and Projection (UMAP) [28] was performed, to identify latent groupings in the data.

2.3. Electrode spacing

A micro-pipette was used to transfer 150 μL from the bottom of the centrifuge tube to three micro-wells with distance between the centres of the bottom electrodes 1.5, 3 and 5 mm, see Fig. 1(d). The electrical potential across the electrodes was recorded according to the parameters in Section 2.2, both with and without illumination (~ 1000 lx from LED lamp on a timer), to explore the effect of electrode spacing on measurements.

2.4. Liquid marbles on flexible open mesh surface

A micro-pipette was used to form droplets (30–150 μL) containing a high density of *C. vulgaris* cells. The droplets were gently rolled across the surface of a variety of hydrophobic powders in polystyrene weighing dishes. As the droplets became encased in a granular coating they formed LMs from 4–6 mm diameter. Fig. 2(a) shows LM with ultra-high-density polyethylene (PE) coating (Sigma-Aldrich, CAS 9002-884, product code 1002018483) average particle size 100 μm . Fig. 2(b) shows LM with polytetrafluoroethylene (PTFE) coating (Alfa Aesar, CAS 900284-0, product code 44184) particle size 6–10 μm . Fig. 2(c) shows LM with hydrophobic silica (SiO_2) coating (Cab-O-Sil, TS-720) average particle size 0.2–0.3 μm (see Appendix C).

LMs (~ 6 mm diameter) were carefully rolled onto open nylon mesh net (1 mm squares) such that the plane of the net deformed under the weight of the LM. Pairs of electrodes (as above), encapsulated inside a plastic tube (~ 10 mm diameter) and held in adjustable height arms were inserted into LM from below, through the holes in the underlying mesh (Fig. 2(d)). The electrical potential across the electrodes was recorded as above.

2.5. Liquid marbles in a machined recess

A recess was machined into a glass-reinforced epoxy laminate (bare FR4 board, 3.14 mm thickness) with a bullnose bit (6.4 mm diameter) to a depth of ~ 2.0 mm. A pair of holes (0.5 mm diameter, 3 mm between centres) were drilled into the bottom of the recess. A pair of electrodes (99.9% pure platinum wire, 0.3 mm diameter) were sealed into the holes with air dry polymerized siloxanes (marine grade silicone sealant) such that the tapered tips of electrodes were flush with the surface of the FR4 board, see Fig. 2(e). LMs (~ 5 mm diameter) were carefully rolled into the recess, which enabled the electrodes to pierce the powder coating into the core, as described previously.

2.6. Liquid marbles in 3D printed recesses

Cylinders (35 mm diameter, 10 mm height) were 3D printed (Ulti-maker, model S5, 0.4 mm nozzle) in polylactic acid (PLA). The cylinder's top surface was profiled to encourage LMs to roll due to gravity and tiling, into hemispherical recess (6 mm diameter). Two or more through-holes (0.6 mm diameter) were positioned symmetrically under the hemispherical recess (Fig. 2(f)).

On the bottom of the cylinder, hemispherical recesses of 1 mm diameter were located at the start of the through-holes to ease electrode insertion. Adhesive was applied to the bottom of the cylinders and a needle inserted from above to mark locations of the holes. The cylinders were held by utility clamps in retort stands and adjusted to level (within one degree of horizontal, by bullseye spirit level). LMs (5–6 mm diameter) were carefully rolled into the recess in the top, see Fig. 2(f).

Electrodes (stainless steel and platinum/iridium subdermal needles, 0.45 mm diameter) were inserted into the holes (from below) such that the tips of electrodes pierced the power coating of LMs. The bases of the needle electrodes were secured with adhesive tack such that their tips were fixed ~ 2 mm above the surface of the cylinder (close to the centre of LM).

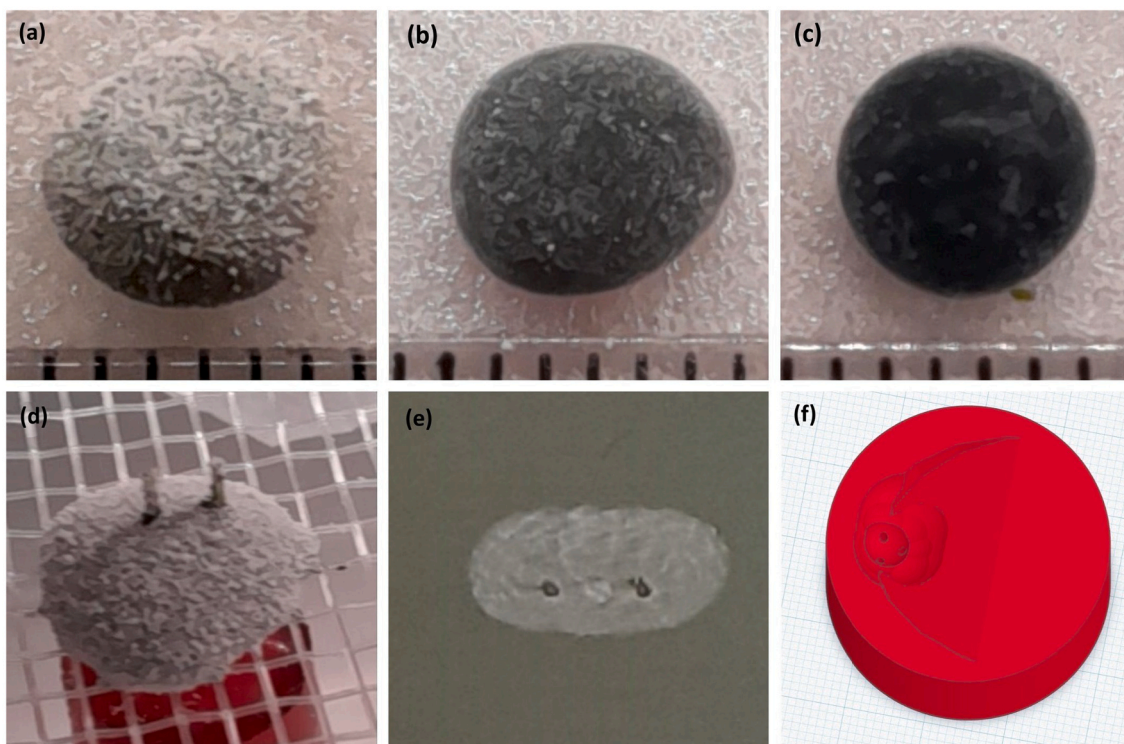


Fig. 2. *C. vulgaris* cells in LM 60 μL with (a) PE coating, (b) PTFE coating, (c) SiO_2 coating (scale in mm), (d) electrodes insert from below into LM with PE coating on mesh, (e) machined recess with embedded electrodes and (f) 3D printed surface with recess for LM and holes to insert electrodes/fibre optics.

2.7. Physical properties of *C. vulgaris* LM

The mechanical robustness of LMs 30–100 μL with PE, PTFE and SiO_2 coatings was evaluated by observing their ability to be manipulated without rupturing.

The optical transparency of 60 μL LMs containing distilled water and *Chlorella* cells in the growth medium, with PE, PTFE and SiO_2 coatings was measured. LMs were carefully rolled into the shallow (ground) recess in the bespoke transparent acrylic stand. A laser beam of wavelength 650 nm was directed into the centre of the LM. Transmitted light was measured with an optical power meter (UNIT-T, model UT385) align (in clamp) on the far side of LM.

Photographs of settled cells inside LMs containing 60 μL of *Chlorella* cells in the growth medium, with SiO_2 coating, were taken periodically (Dino-Lite, model AM7115MZW and Samsung, A20). LMs were positioned in the centre of semi-transparent, flat, polystyrene weighing boat and hemispherical recess in transparent acrylic sheet. A white LED (5 mm diameter, ~ 2.5 lx) was located beneath and illuminated when photographed.

Separate measurements of the electrical conductivity of de-ionised water and *Chlorella* cells in growth medium were recorded with conductivity meter (HM Digital Inc, model COM-100).

The use of fibre optics to bypass the light attenuation of powder coating shell on LM was explored. A taper (similar to the end of a hypodermic needle tip) was added to the end of the fibre cable (with a micro-shear cutter) to minimise disruption of the powder particles when inserted into the core.

3. Results

3.1. Response to light in micro-wells with two pairs of electrodes

A representative example of potential across ‘bottom’ and ‘top’ electrodes, with 3 mm between centres, is shown in Fig. 3. The ‘bottom’ electrode pair shows typical spiking behaviour, whose amplitude is approximately 12.5 mV and correlates with periodic illumination (~ 1000 lx) of approximately 15 min h^{-1} .

The voltage recorded across the top electrodes was significantly smaller in magnitude approximately 0.2 mV and also correlates with the periodic illumination. Possible causes of this small voltage are (1) electrical conductive through the body of the liquid ($\sim 2500 \mu\text{S/cm}$) combined with electrode pairs not exactly orthogonal to each other and (2) potential voltage gradient across the body of the liquid due to illuminated *Chlorella* cells in suspension.

3.2. Effect of electrode spacing

Exemplar traces from micro-wells with 1.5, 3.0 and 5.0 mm electrode spacing are shown in Fig. 4. Potential across electrodes with 3 mm between centres typically varied by ~ 5 mV, 3 mm by ~ 4 mV and 1.5 mm by ~ 0.3 mV. All three potentials correlate with illumination at approximately 15 min h^{-1}

Descriptive statistics on data for the three-electrode spacings are shown in Table 1. Neither spike duration nor amplitude datasets for any electrode spacing were normally distributed (data not shown). More variation was observed in both spike duration and amplitude measurements for 3 mm spaced electrodes, but significantly more spikes were identified in these experiments ($p < 0.001$). Kruskal-Wallis tests demonstrated that there was a significant difference between medians for spike amplitude ($p < 0.001$) for the 3 mm spaced electrodes, and a significant difference between spike duration ($p = 0.003$), with 5 mm spacing. No spikes were identified in control experiments (data not shown).

Fig. 5 shows UMAP embeddings for all measurement data, projected into two dimensions. Visual inspection of these clusters supports the statistical observations in that data naturally fall into three clusters (using a minimum cluster boundary of 5.0), with the largest cluster (for 3 mm spaced electrodes) having more variation. Interestingly, all clusters also appear to form at least two natural sub-clusters, and the largest of the three main clusters appears to have three or four; this indicates that multiple types of phenomenon, or multiple modes of the same phenomenon, may have been measured. Three dimensional projections were consistent with the two dimensional (data not shown).

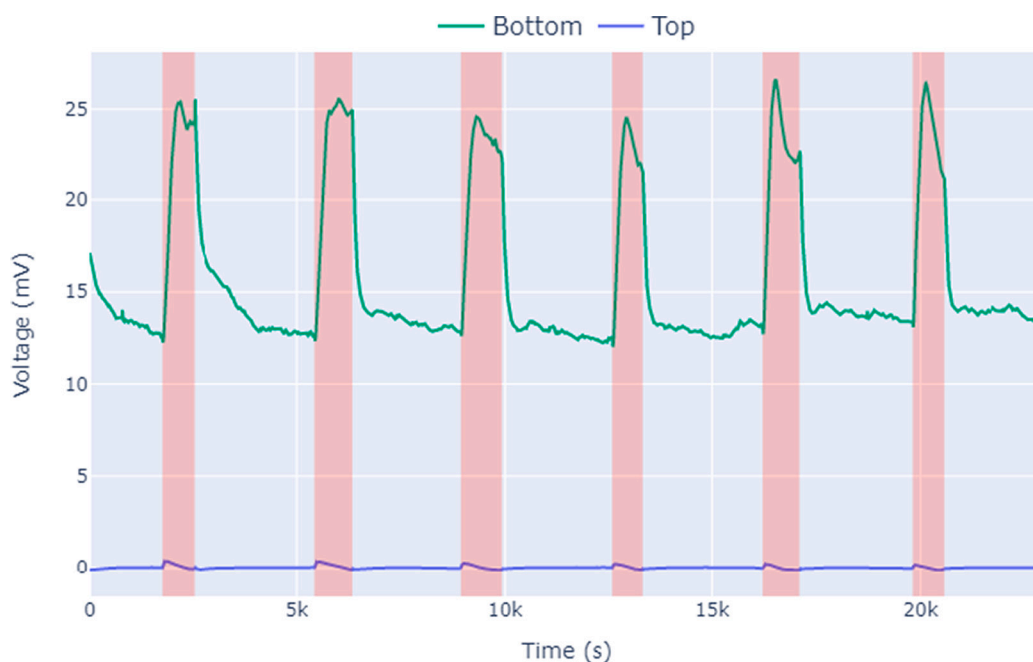


Fig. 3. Representative electrical potential measurements from a *Chlorella*-filled micro-well, via two pairs of electrodes, each with 3 mm separation. Red shaded regions indicate periods when illumination was provided. (For interpretation of the references to color in this figure legend, the reader is referred to the web version of this article.)

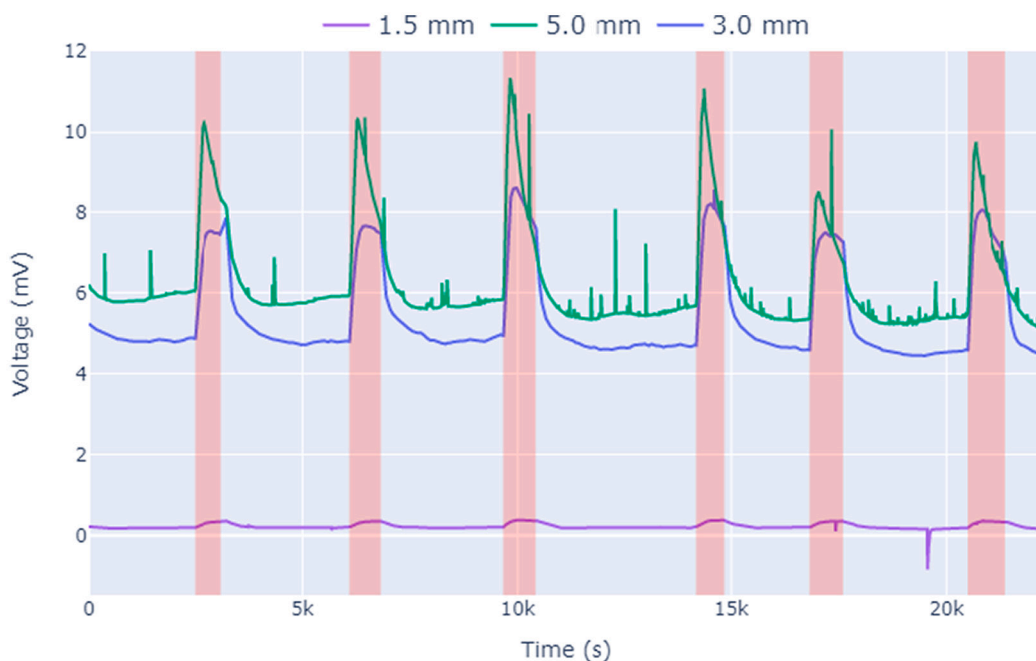


Fig. 4. Three micro-wells with distance between centres of ‘bottom’ electrodes: 1.5 mm, 3 mm and 5 mm. Red shaded regions indicate periods when illumination was provided. (For interpretation of the references to color in this figure legend, the reader is referred to the web version of this article.)

Table 1

Descriptive statistics on electrical potential recordings, for three electrode spacings in micro-well experiments. *Med*: median, *IQR*: interquartile range, *: significant difference at $p < 0.01$, via Kruskal-Wallis test, †: significant difference at $p < 0.001$, via Chi Square test.

		1.5 mm	3.0 mm	5.0 mm
Spike duration (s)	<i>Med</i>	1361	1629	2134*
	<i>IQR</i>	1667	4855	1722
Spike amplitude (mV)	<i>Med</i>	1.263	19.21*	4.371
	<i>IQR</i>	1.435	35.58	15.30
<i>n</i> spikes	Total	100	204†	119

3.3. LM electrical measurements

Our experiments showed that LMs in various experimental environments also support the generation and subsequent measurement of spiking behaviour, with amplitudes measuring in millivolts and wavelengths in the order of thousands of seconds. Electrical spikes initiated in LMs illuminated with ambient light are shown in Figs. 6, 7 and 8.

Fig. 6 shows an exemplar recording of electrical activity in an LM shaped by flexible mesh. The duration is ~1400 s and amplitude ~7 mV. Similar activity was not recorded in LM on flat surfaces.

Fig. 7 shows a representative spike with a duration of ~6000 s and 4 mV peak amplitude, measured from a LM in a machined recess with electrode spacing of 3 mm).

Fig. 8(a and b) shows representative electrical activity recorded

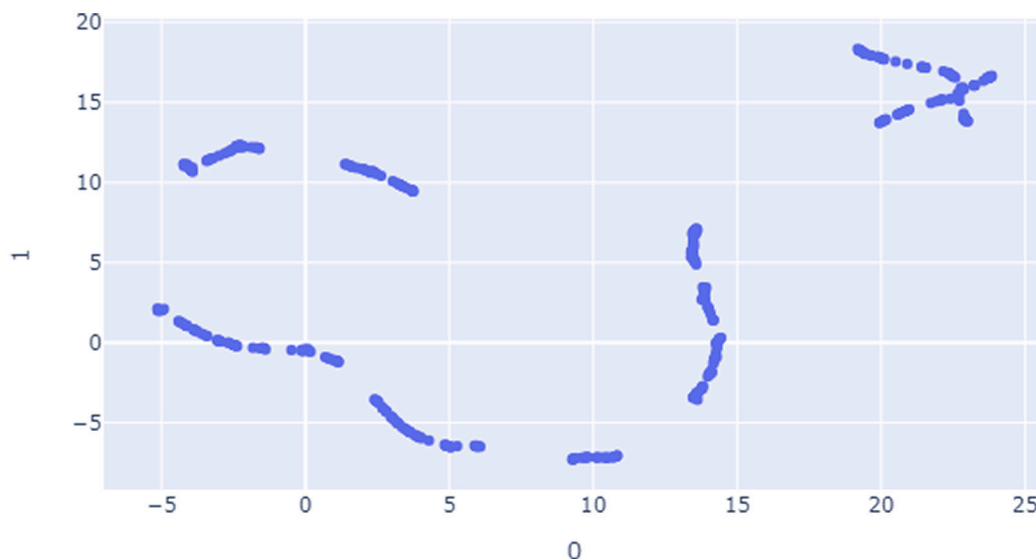


Fig. 5. UMAP projections for all micro-well measurements. Three natural clusters are present, with each appearing to form at least two distinct sub-clusters. Note that axes here are relative and dimensionless.

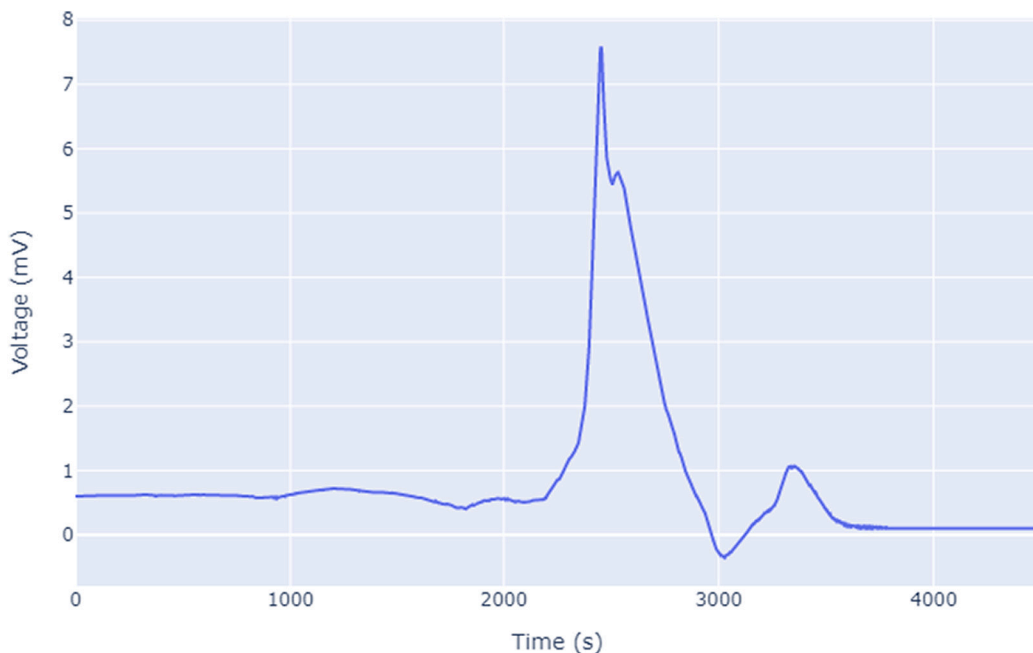


Fig. 6. LM on nylon mesh, Pt electrodes with 2 mm spacing inserted from below.

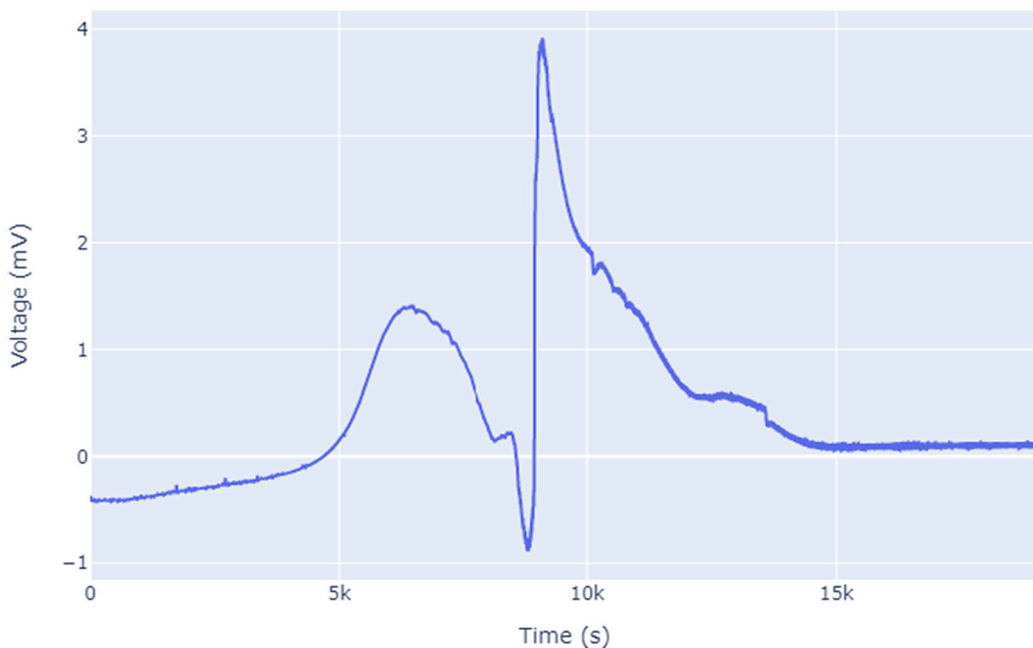


Fig. 7. LM in machined recess with Pt electrodes.

between two and three Pt/Ir electrodes, in LMs containing *C. vulgaris* cells in 3D printed recess.

3.4. Physical properties of *C. vulgaris* LM

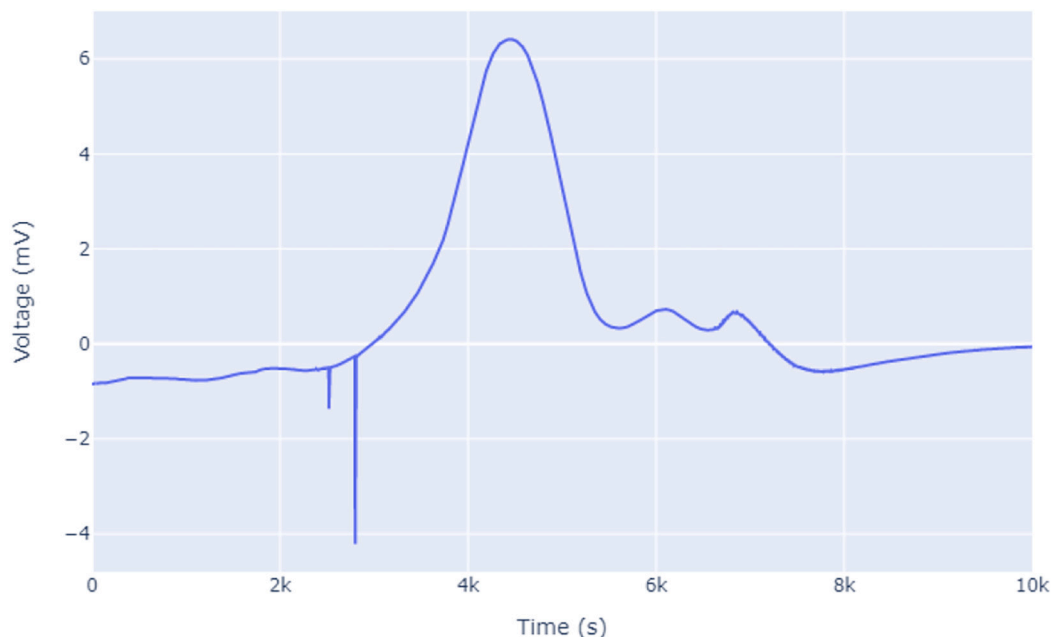
It was observed that the mechanical robustness of LMs was affected by:

- Physical size - LMs larger than ~5 mm in diameter required careful handling to avoid rupturing of the powder shell.

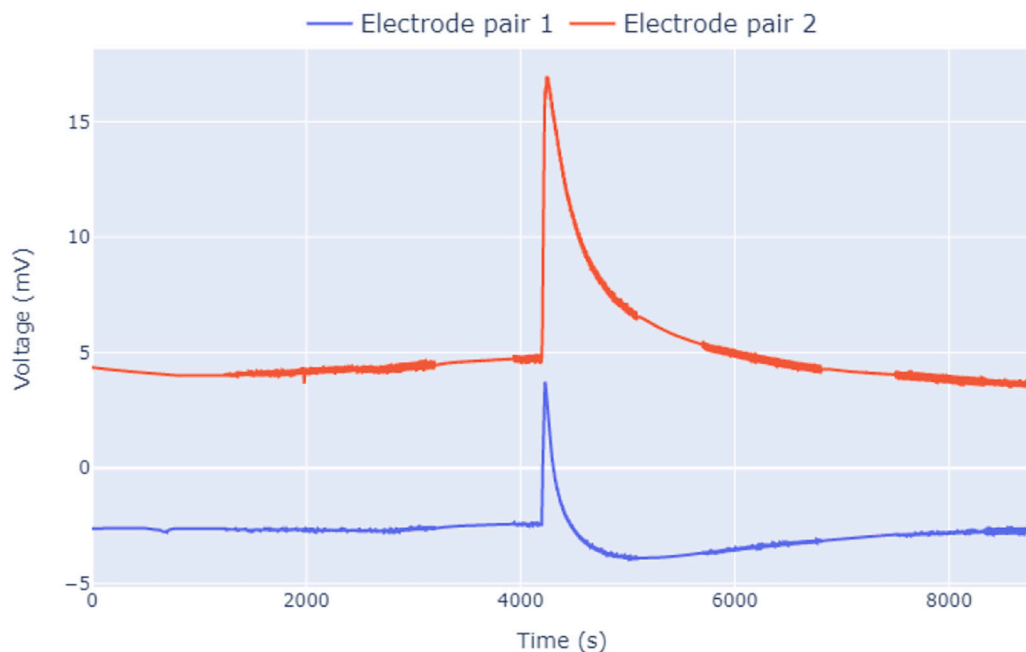
- Material properties of powder coating - PE coating was mechanically more robust than PTFE coating which was more robust than SiO₂ coating.
- The surface which the LM rests on can indirectly affect overall robustness

The optical attenuation of light passing through LMs containing *C. vulgaris* cells was observed to be affected by the material properties of powder shell:

- PE ~99.4% (650 nm)
- PTFE ~99.5% (650 nm)



(a)



(b)

Fig. 8. LM (60 μ L, PE coating) in 3D printed recess: (a) two Pt/Ir electrodes with 3 mm spacing and (b) three Pt/Ir electrodes with 3 mm spacing.

SiO₂ ~95.3% (650 nm)

On flat rigid surfaces, the cells inside LM (60 μ L, SiO₂ coating) initially appeared uniformly distributed, see Fig. 9(a). However, after 30 min the cells had settled non-uniformly on the bottom of LM, see Fig. 9(b). For LM (60 μ L, SiO₂ coating) on 3 mm diameter recess, the cells initially appeared evenly dispersed (Fig. 9(c)). After 30 min the cells had mostly settled above 3 mm diameter recess (off-centre relative

to LM centre) (Fig. 9(d)).

The electrical conductivity of the de-ionised water used in experiments was ~2.7 μ S/cm and Chlorella cells in the growth medium was ~2500 μ S/cm. The high salt content of the growth medium was the reason for this increased conductivity, which permitted making electrical measurements with no current injection.

Carefully inserting a thin (external diameter 0.9 mm, fibre diameter 125 μ m) fibre optic cable through the coating of LM allowed the core of

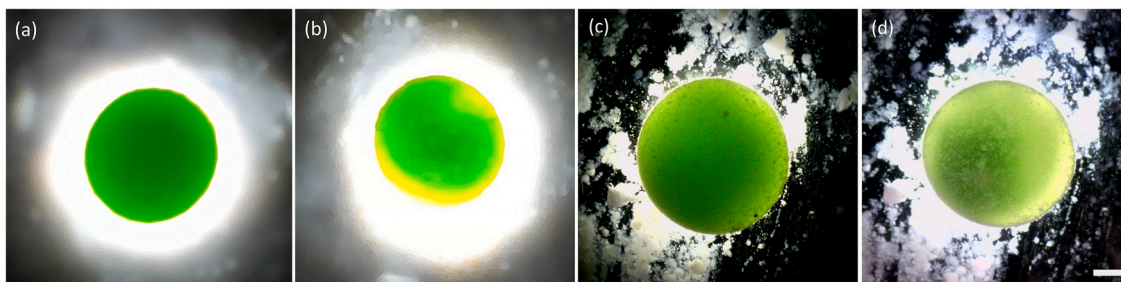


Fig. 9. *C. vulgaris* LM (60 μ L, SiO₂ coating) with LED beneath: (a) initial distribution of cells with LM on flat surface, (b) distribution after 30 min on flat, (c) initial cell distribution with LM on 3 mm diameter recess and (d) cell distribution after 30 min on recess. Scale bar: 1 mm.

LM to be illuminated without the attenuation losses of going through the powder coating. The fibre optic cable was integrated (with electrodes) into the design of 3D printed recess. Recording of electrical activity with illumination were with external light sources rather than fibre optic cable.

4. Discussion

A strong response to illumination was observed between ‘bottom’ electrodes in contact with layer of *C. vulgaris* cells and growth medium. No significant response was recorded between ‘top’ electrodes in contact with the growth medium. This indicates that electrical activity emanates from *C. vulgaris* cells when illuminated [29–31].

4.1. Electrode spacing optimisation

Electrical potential was observed to vary with electrode separation. A distance of \sim 3 mm between centres of electrodes was found to be effective for monitoring electrical activity, as was evidenced by the identification of significantly more and larger spikes in the recordings. Data for 3 mm separated electrodes were more variable than other categories despite more spikes being detected, which indicates that this separation is also able to detect a wider range of spiking events. This suggests that there is an optimum spacing for the electrodes in any environment which is likely to be related to the phenomena being measured (here, the liberation of hydrogen ions, electrons and gaseous oxygen as byproducts of the reactions involved in photosynthesis) and the geometry of the testing environment, possibly due to the generation and interaction of complex reaction-diffusion wavefronts.

Clustering analysis indicated that results naturally form distinct clusters for each electrode spacing, but furthermore, distinct sub-clusters were identified. While the techniques used here cannot be used to link cause and effect, we may speculate that multiple phenomena or types of the same phenomenon were identified with this measurement apparatus, e.g. photosynthetic waves in multiple modalities of environmental illumination. This may be investigated further with exclusion experiments combined with appropriate statistical measurements (e.g. autocorrelation). Crucially, more sub-clusters were identified in the 3 mm category, hence we may further suggest that this spacing was optimal for identifying more types of bioelectrical patterns.

4.2. LM measurement optimisation

In LMs, the continuity of a cell layer across the bottom of the measurement environment is restricted by the number of cells enclosed by powder coating, which has knock-on implications for the mechanics of making electrical measurements. The following demonstrates a mathematical description for designing optimal measurements.

A LM of 6 mm diameter, with 1×10^6 *C. vulgaris* cells per ml, holds $\sim 1.1 \times 10^6$ cells. The average Chlorella cell diameter is ~ 4.5 μ m, so each cell has a volume 4.77×10^{-11} ml, hence a total volume of cells in

this environment of ~ 0.49 μ L. Random packing of equal spheres has a density of around 64%, so the volume occupied by cells increases to ~ 0.76 μ L. Cell layer thickness depends on base area which depends on LM shape. On flat surfaces, LMs of 6 mm diameter deform to approximate shape of hemisphere which increases diameter to ~ 7.49 mm diameter, see Fig. 10(a). Average cell layer thickness ~ 0.017 mm.

If LM is ‘pressed’ into a spherical shape by placing in hemispherical recess (of similar diameter), see Fig. 10(b), the maximum cell layer thickness can be increased to ~ 0.03 mm in the middle. However, the layer thickness decreases near the electrodes with a chord length of only ~ 2.57 mm, which is insufficient to encompass electrodes. The spread of the cell layer can be widened to include the electrodes by changing from circular (Fig. 10(c)) to oval recess (Fig. 10(d)) such that settled cells form a contiguous link between the electrodes.

4.3. LM immobilisation technique

3D printing of recess for LM and positional supports for electrodes and fibre optics was found to be practical and advantageous. The flexibility of 3D printing allowed LM geometry and separation between electrodes/fibre to be quickly and accurately adjusted as desired. The 3D printer used (Ultimaker S5) struggled with the formation of small holes (less than 0.6 mm diameter with 0.4 mm nozzle) so manual finishing (hole clearing with 0.5 mm dia drill bit) was required. The insertion of pair or triple electrodes/fibre into LM of ~ 6 mm diameter can be achieved with ~ 3 mm separation. However, if more than three electrodes and/or fibres are required their separation needs to be reduced.

The variability of electrical activity recorded in LMs (data not shown) was found to be greater than in micro-well; ongoing research to quantify the characterise of LM sensors will be reported in due course. Regardless, we find that LMs support making measurements comparable to those in more conventional, rigid and impermeable environments.

4.4. Physical properties of LMs

SiO₂ coating is optically approximately 7 times more transparent than PE and PTFE. Therefore, SiO₂ is an advantageous coating for *C. vulgaris* LM optical sensors. The optimal physical size of LM for use as a sensor is a balance between the mechanical robustness of powder coating (smaller is desirable) and sufficient separation between electrodes/fibre optics for good electrical measurements (larger is desirable). In the case of two-needle electrodes, LM diameter of c. 5 mm was found to be workable. In the case of three insertions (three-needle electrodes, two-needle electrodes and fibre optic) a larger LM diameter of c. 6 mm is beneficial. The latter was problematic without a powder coating with suitable mechanical properties (e.g. PE).

The salts in the growth medium increase the electrical conductivity of the solution by approximately three orders of magnitude (from ~ 2.7 μ S/cm to ~ 2500 μ S/cm) so electrical potentials dissipate quicker.

We described in previous publications the various benefits of using LMs as an environment for sensing media, which include gas

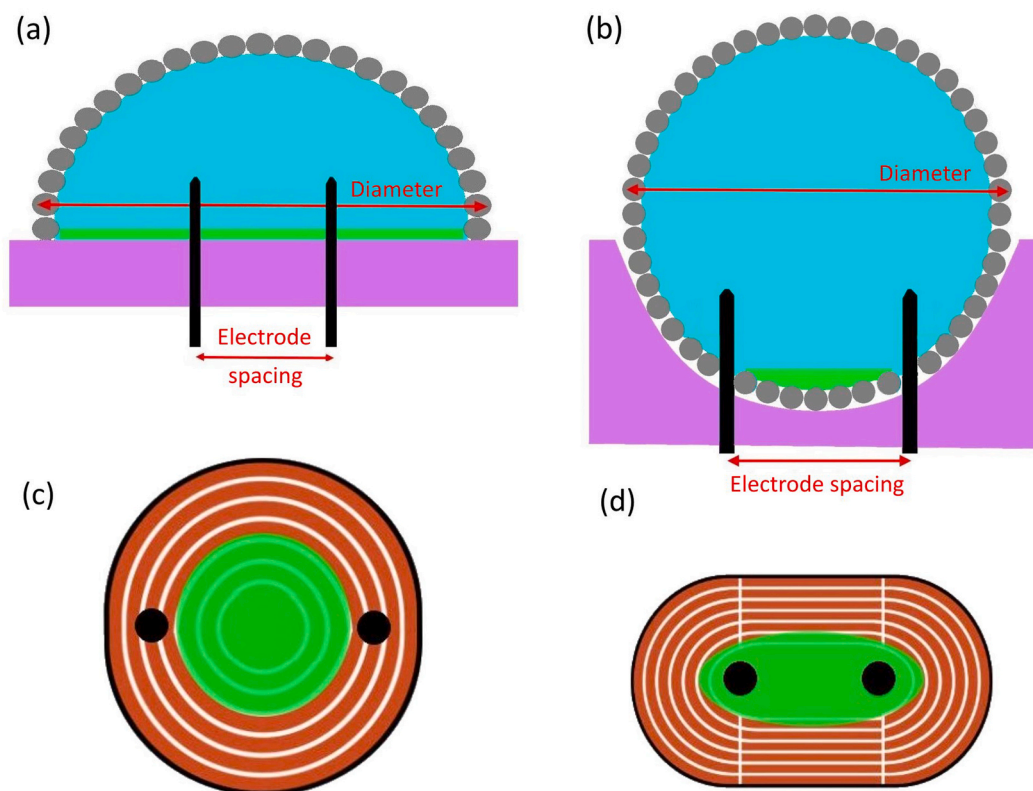


Fig. 10. LMs on (a) flat surface, (b) recessed surface, (c) settled cells in symmetrical recess and (d) settled cells in oval recess.

permeability, the potential for fusion with other LMs and their supporting three-dimensional electro-chemical wave phenomena. We observe in Figs. 6–8 that action potential-like events are observed that were not pronounced in micro-well experiments; the mechanics underlying this are unclear but add potential richness to any recordings made via this method.

The optical attenuation of most powder coatings on LMs is extremely high therefore external illumination of the core is challenging. Using a fibre optic cable to bypass the coating can be a more efficient technique which allows the core to be illuminated without excessive heating.

5. Conclusions

Chlorella dispersed in both rigid micro-wells and LMs shows periodic electrical activity in the form of spikes. Measured electrical activity is responsive to light irradiation, hence indicating the suitability of these experimental environments for photosensing applications. The exact response characteristics of such Chlorella sensors can be adjusted by changing the experimental environment; LM coating shape is a governing parameter in how the cells settle/distribute within the core. Further, sensor responsivity is influenced by electrode separation. The ability to control LM geometry using 3D printed recess has been demonstrated. Optical attenuation by the coating can be mitigated through the insertion of fibre optics into the core. The versatility of LMs, in terms of being able to tailor the encapsulated micro-organisms and coating, provides a promising opportunity for the development of unconventional computing systems. Algae liquid marbles used as electro-optical sensors has not been previously published.

Declaration of Competing Interest

The authors (Neil Phillips, Richard Mayne and Andrew Adamatzky) declare that they have no conflict of interests.

Acknowledgements

This research was supported by the Engineering and Physical Sciences Research Council (EPSRC), UK with grant EP/P016677/1 ‘Computing with Liquid Marbles’. This work was conducted entirely at the University of the West of England, Bristol, UK.

Appendix A. *C. vulgaris* culture

A culture of *C. vulgaris* cells was maintained with Bold Modified Basal on a prolonged basis in an open, glass aquarium of 10 l capacity (W 180, L 340, H 210 mm, manufactured by Aquatlantis Aquarium Ltd, model Explorer Madrid). Periodically illuminated (16 hours ‘on’ and 8 hours ‘off’) with LED growth lamp (120 W input power) suspended 300 mm above the surface of the water. The water was continuously circulated with a submerged electric pump (model YB-50, maximum rated flow rate 600 l h⁻¹, input power 9 W). After the *C. vulgaris* was established the tank was aerated (to maintain carbon dioxide level in water) with an airstone supplied with compressed air at flow rate of 0.4 l m⁻¹ (Hailea ACO-9601 set to minimum output). ~25% of water was removed weekly and replaced with fresh growth medium. Over prolonged periods (3 months) unwanted dead cells can accumulate at the bottom of the growth tank and should be removed.

The density of *C. vulgaris* cells was measured microalgae culture density measurer (manufactured by Florida Aqua Farms Inc, model AC-DM9) based on the Secchi principle. A white dot mounted on a calibrated plastic stick is lowered into the growth tank (with pumps switched off) until the dot disappears. Depth is recorded off the scale and approximate cell density is obtained from the density conversion chart provided by manufacturer.

Appendix B. Increasing cell density

C. vulgaris in growth medium (with a cell density of ~10 × 10⁶ cells

per ml) was poured into 50 ml Falcon type tubes, evenly distributed in MSE Centaur 2 centrifuge (fixed arm head, 130 mm radius) and spun at 1500 rpm subjecting the cells to ~ 327 g for 300 s. The top ~ 45 ml of liquid was carefully poured out of tubes leaving the cells in bottom ~ 5 ml, increasing the average cell density of the remaining liquid to $\sim 1 \times 10^8$ cells per ml. A micro-pipette was used to transfer 150 μ l from the bottom of the 5 ml to further increasing the cell density to $\sim 5 \times 10^8$ cells per ml.

Appendix C. Hydrophobic silica

Cab-O-Sil TS-720 is an amorphous fumed silica powder manufactured by Cabot Corporation, USA and distributed in the UK by Innoxia Ltd. The molecular structure consists of nanometre droplets of amorphous silica fused into branched chains. The fumed silica has been surface modified with polydimethylsiloxane. The treatment renders it extremely hydrophobic, with different properties to untreated silica. The supplied powder was thoroughly ground with a pestle and mortar before use. Datasheet: <https://polymerinnovationblog.com/wp-content/uploads/2018/06/Datasheet-CAB-O-SIL-TS720pdf.pdf>.

References

- [1] H. Kitano, F. Matsuno, Biological robustness, in: SICE Annual Conference, 2008, p. 9, <https://doi.org/10.1109/SICE.2008.4654600>.
- [2] G. Xu, W. Shen, X. Wang, Applications of wireless sensor networks in marine environment monitoring: a survey, *Sensors* 14 (9) (2014) 16932–16954, <https://doi.org/10.3390/s140916932>.
- [3] M.J. Moreno-Lizaranzu, F. Cuesta, Improving electronic sensor reliability by robust outlier screening, *Sensors* 13 (10) (2013) 13521–13542, <https://doi.org/10.3390/s131013521>.
- [4] F. Delaine, B. Lebalant, H. Rivano, In situ calibration algorithms for environmental sensor networks: a review, *IEEE Sens. J.* 19 (15) (2019) 5968–5978, <https://doi.org/10.1109/JSEN.2019.2910317>.
- [5] J.B. Coble, R.M. Meyer, P. Ramuhalli, L.J. Bond, H. Hashemian, B. Shumaker, D. Cummins, Review of Sensor Calibration Monitoring for Calibration Interval Extension In Nuclear Power Plants, 2012, <https://doi.org/10.2172/1061413>.
- [6] G. Mills, G. Fones, A review of in situ methods and sensors for monitoring the marine environment, *Sens. Rev.* 32 (2012) 17–28, <https://doi.org/10.1108/02602281211197116>.
- [7] A. Antonacci, V. Scognamiglio, Biotechnological advances in the design of algae-based biosensors, *Trends Biotechnol.* 38 (3) (2020) 334–347, <https://doi.org/10.1016/j.tibtech.2019.10.005>.
- [8] R. Brayner, A. Couté, J. Livage, C. Perrette, C. Sicard, Micro-algal biosensors, *Anal. Bioanal. Chem.* 401 (2) (2011) 581–597, <https://doi.org/10.1007/s00216-011-5107-z>.
- [9] E.J. Stewart, Growing unculturable bacteria, *J. Bacteriol.* 194 (16) (2012) 4151–4160, <https://doi.org/10.1128/JB.00345-12>.
- [10] S. Mhl, B. Beyer, Bio-organic electronics-overview and prospects for the future, *Electronics* 3 (3) (2014) 444–461, <https://doi.org/10.3390/electronics3030444>.
- [11] J. Forth, P.Y. Kim, G. Xie, X. Liu, B.A. Helms, T.P. Russell, Building reconfigurable devices using complex liquid-fluid interfaces, *Adv. Mater.* 31 (18) (2019) 1806370, <https://doi.org/10.1002/adma.201806370>.
- [12] L. Krienitz, V.A. Huss, C. Bock, 125 years of the green survivalist, *Trends Plant Sci.* 20 (2) (2015) 67–69, <https://doi.org/10.1016/j.tplants.2014.11.005>.
- [13] R. Allaguvatova, Y. Myasina, V. Zakharenko, L. Gaysina, A simple method for the cultivation of algae *Chlorella vulgaris* Bejerinck 390 (012020) (2019), <https://doi.org/10.1088/1755-1315/390/1/012020>.
- [14] B. De Caprariis, P. De Filippis, A. Di Battista, L. Di Palma, M. Scarsella, Exoelectrogenic activity of a green microalgae, *Chlorella vulgaris*, in a bio-photovoltaic cells (bpvs), *Chem. Eng. Trans.* 38 (2014), <https://doi.org/10.3303/CET1438088>.
- [15] H. Helisch, J. Keppeler, G. Detrell, S. Belz, R. Ewald, S. Fasoulas, A. Heyer, High density long-term cultivation of *Chlorella vulgaris* sag 211-12 in a novel microgravity-capable membrane raceway photobioreactor for future bioregenerative life support in space, *Life Sci. Space Res.* (2020), <https://doi.org/10.1016/j.lssr.2019.08.001>.
- [16] R. Rossi, E. Camargo, P. Crnkovic, A. Lombardi, Physiological and biochemical responses of *Chlorella vulgaris* to real cement flue gas under controlled conditions, *Water, Air Soil Pollut.* 229 (259) (2018), <https://doi.org/10.1007/s11270-018-3914-y>.
- [17] C. Sorokin, R. Krauss, Maximum growth rates of *Chlorella* in steady-state and in synchronized cultures, *PNAS* 45 (12) (1959) 1740–1744, <https://doi.org/10.1073/pnas.45.12.1740>.
- [18] T.C. Draper, N. Phillips, R. Weerasekera, R. Mayne, C. Fullarton, B.P.J. de Lacy Costello, A. Adamatzky, Contactless sensing of liquid marbles for detection, characterisation and computing, *Lab Chip* 20 (2020) 136–146, <https://doi.org/10.1039/C9LC01001G>.
- [19] C. Fullarton, T.C. Draper, N. Phillips, B.P.J. de Lacy Costello, A. Adamatzky, Belousov-zhabotinsky reaction in liquid marbles, *J. Phys.: Mater.* 2 (1) (2019) 015005, <https://doi.org/10.1088/2515-7639/aaed4c>.
- [20] A. Adamatzky, C. Fullarton, N. Phillips, B. De Lacy Costello, T.C. Draper, Thermal switch of oscillation frequency in belousov-zhabotinsky liquid marbles, *Royal Soc. Open Sci.* 6 (4) (2019) 190078, <https://doi.org/10.1098/rsos.190078>.
- [21] T.C. Draper, C. Fullarton, N. Phillips, B.P. de Lacy Costello, A. Adamatzky, Liquid marble interaction gate for collision-based computing, *Mater. Today* 20 (10) (2017) 561–568, <https://doi.org/10.1016/j.mattod.2017.09.004>.
- [22] T.C. Draper, C. Fullarton, N. Phillips, B.P.J. de Lacy Costello, A. Adamatzky, Scientific Reports, 2018, <https://doi.org/10.1038/s41598-018-32540-w>.
- [23] N.-T. Nguyen, M. Hejazian, C.H. Ooi, N. Kashaninejad, Recent advances and future perspectives on microfluidic liquid handling, *Micromachines* 8 (6) (2017), <https://doi.org/10.3390/mi8060186>.
- [24] N.-K. Nguyen, P. Singha, J. Zhang, H.-P. Phan, N.-T. Nguyen, C.H. Ooi, Digital imaging-based colourimetry for enzymatic processes in transparent liquid marbles, *Chem. Phys. Chem.* 22 (1) (2021) 99–105, <https://doi.org/10.1002/cphc.202000760>.
- [25] T. Arbatan, L. Li, J. Tian, W. Shen, Liquid marbles as micro-bioreactors for rapid blood typing, *Adv. Healthcare Mater.* 1 (1) (2012) 80–83, <https://doi.org/10.1002/adhm.201100016>.
- [26] T.C. Draper, M. Dueñas-Díez, J. Pérez-Mercader, Exploring the symbol processing 'time interval' parametric constraint in a belousov-zhabotinsky operated chemical Turing machine, *RSC Adv.* 11 (2021) 23151–23160, <https://doi.org/10.1039/D1RA03856G>.
- [27] P. Virtanen, R. Gommers, T.E. Oliphant, M. Haberland, T. Reddy, D. Cournapeau, E. Burovski, P. Peterson, W. Weckesser, J. Bright, S.J. van der Walt, M. Brett, J. Wilson, K.J. Millman, N. Mayorov, A.R.J. Nelson, E. Jones, R. Kern, E. Larson, C. J. Carey, I. Polat, Y. Feng, E.W. Moore, J. VanderPlas, D. Laxalde, J. Perktold, R. Cimrman, I. Henriksen, E.A. Quintero, C.R. Harris, A.M. Archibald, A.H. Ribeiro, F. Pedregosa, P. van Mulbregt, SciPy 1.0 Contributors, SciPy 1.0: Fundamental Algorithms for Scientific Computing in Python, *Nat. Methods* 17 (2020) 261–272, <https://doi.org/10.1038/s41592-019-0686-2>.
- [28] L. McInnes, J. Healy, N. Saul, L. Groberger, Uniform manifold approximation and projection, *J. Open Source Software* 3 (29) (2018) 861, <https://doi.org/10.21105/joss.00861>.
- [29] E.-H. Lee, S.-W. Lee, R.F. Saraf, Noninvasive measurement of membrane potential modulation in microorganisms: Photosynthesis in green algae, *ACS Nano* 8 (1) (2014) 780–786, <https://doi.org/10.1021/nn405437z>.
- [30] C.-C. Fu, T.-C. Hung, W.-T. Wu, T.-C. Wen, C.-H. Su, Current and voltage responses in instant photosynthetic microbial cells with *Spirulina platensis*, *Biochem. Eng. J.* 52 (2) (2010) 175–180, <https://doi.org/10.1016/j.bej.2010.08.004>.
- [31] F.-L. Ng, S.-M. Phang, M. Iwamoto, T. Manaka, C.-H. Thong, K. Shimomura, V. Periasamy, G.G. Kumar, K. Yunus, A.C. Fisher, Algal biophotovoltaic devices: Surface potential studies, *ACS Sustain. Chem. Eng.* 8 (28) (2020) 10511–10520, <https://doi.org/10.1021/acssuschemeng.0c02831>.